INVESTIGATION OF TEMPERATURE HOMOGENEITY DURING INFRARED SOLDERING OF SILICON SOLAR CELLS USING THE FINITE ELEMENT METHOD

Daniel C. Joseph[1,*], Angela De Rose[1], Dirk Eberlein[1], Onur Parlayan[1], Benjamin Grübel[1], Andreas J. Beinert[1] and Holger Neuhaus[1]
[1] Fraunhofer Institute for Solar Energy Systems ISE, Heidenhofstrasse 2, 79110 Freiburg, Germany
*Corresponding author: e-mail to: daniel.christopher.joseph@ise.fraunhofer.de

ABSTRACT: In the production of silicon photovoltaic modules, copper ribbons are connected to the electrodes of solar cells using infrared soldering through automated stringer machines. Despite its efficiency and high throughput, infrared soldering results in inhomogeneous heating of the solar cells. Accurately measuring the solar cell temperature during the soldering process within the stringer poses a significant challenge, hindering process optimization to reduce this inhomogeneity. This study presents a novel finite element model to simulate the infrared soldering process, which calculates the solar cell temperature based on factors such as the applied electrical power, the radiation duration from the infrared emitters, and the hotplate temperature. The model is validated using thermocouple measurements at various points on the solar cells during the soldering process, showing a maximum difference of (8 ± 4) K in the peak temperature region between the simulation and experimental data. This FEM model can easily be adapted to new solar cell technologies and various solar cell sizes. Thus, a robust finite element model is developed to accurately determine the solar cell temperature during the infrared soldering process.

Keywords: Finite element method, Infrared soldering, Photovoltaic modules, Radiative heat transfer, Interconnection, Solar cells

1 INTRODUCTION

The soldering process plays a critical role in ensuring both electrical connectivity and mechanical stability in photovoltaic (PV) modules. Precise and homogeneous heating of the solar cells during this process is essential to reduce the thermomechanical stress and ensure the reliability of PV modules [1, 2]. In the photovoltaic industry, automated stringer machines are primarily used to perform industrial soldering processes using infrared (IR) radiation [3] .

Despite its advantages, such as rapid non-contact heating, the IR soldering process results in an inhomogeneous temperature distribution on the solar cells due to the uneven heat distribution and shading effects of the down-holder. This inhomogeneity leads to issues such as badly or non-contacted joints and solar cell overheating. However, measuring the exact solar cell temperature during the soldering process within the stringer presents a complex challenge.

The aim of this study is to develop a finite element method (FEM) model of the industrial IR soldering process used in the PV industry. This model is designed to compute the temperature distribution on industrial silicon solar cells during the IR soldering process. The model aims to enhance the accuracy of temperature predictions during the IR soldering process, thereby contributing to the optimization of the soldering procedure. This model is validated through temperature measurements taken at various positions on passivated emitter and rear cells (PERC) half-cells during the IR soldering process in a stringer. Furthermore, the model is adaptable, enabling temperature calculations for various solar cell technologies, such as TopCon and silicon heterojunction (SHJ), and different solar cell sizes.

2 METHODS

2.1 Infrared soldering

Infrared soldering by industrial stringer utilizes radiative heat transfer [3–5] that operate in the wavelength range of 0.5 to 3 μm [6]. Figure 1 sketches schematically the hotplates and an IR heating zone used in a stringer. The solar cells and the interconnecting wires are held in position by the down-holder during the IR soldering process. The hotplates before the IR heating zones are used to pre-heat the solar cells and the interconnections, while the hotplates after the IR heating zones are used to control the cooling of the soldered solar cells. Each IR zone contains four IR emitters that radiate infrared radiation to heat the solar cells and solder coated copper ribbon.

An IR emitter in the industrial stringer comprises a quartz halogen tube with an internal tungsten filament. The tungsten filament within the emitter is heated by the Joule heating effect [7]. The IR emitters have an efficiency of 90–95 % and exhibit a rapid response to changes in heating [8, 9]. The temperature of the tungsten filament can be regulated using the electric power supplied to the filament (P_{IR}) and the duration of current flow (t_{IR}). These parameters, P_{IR} and t_{IR}, along with the hotplate temperature T_{HP}, are used to control the solar cell temperature and will be referred to as process parameters.

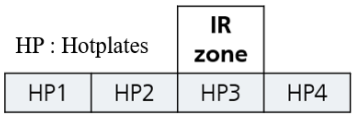

Figure 1 : Hotplates and IR zone position considered for the FEM model.

2.2 FEM Model

The objective of predicting solar cell temperature during the IR soldering process in an industrial stringer is achieved using finite element method (FEM) modeling in COMSOL Multiphysics 6.2. The FEM model consists of the IR emitters, featuring a simplified representation of the tungsten filament, the solar cell with the ribbons and down-holder. The temperature of the tungsten filament (T_F), incorporating process parameters P_{IR} and t_{IR}, is used as the input conditions for this FEM model. The transient temperature of the filament depends on the process parameters P_{IR} and t_{IR}. Temperature-dependent material properties for the tungsten filament, are obtained from [10, 11]. In this FEM model, the temperature values T_F are

utilized to calculate the radiation emitted from the IR emitters. Using these radiation values, the solar cell temperature (T_C) is computed through heat transfer in solids and surface-to-surface radiation physics. This process models the radiative heat transfer between the IR emitters and the solar cells with ribbons.

Table I : Thermal properties of the various components used for the simulation.

Material	Thermal conductivity, k [W/m*K]	Specific heat capacity, C_p [J/kg*K]
Silicon solar cell	130†	700†
Sn60Pb40 solder	50†	150†
Copper wire	400‡	385‡
Down-holder	238†	900†
Tungsten filament	k(T) [10]	C_p(T) [10]
Aluminum reflector	238‡	900‡
Quartz glass	1.4‡	730‡

Table II : Optical properties of the various components.

Material	Emissivity, ε [-]	Reflectivity, ρ [-]
Silicon solar cell	0.70 †	0.13†
Sn60Pb40 solder	0.30 [12]	1 - ε
Copper wire	0.15 [12]	
Down-holder	0.30†	
Tungsten filament	ε(T) [11]	
Aluminum reflector	1 - ρ	0.92‡
Quartz glass	0.08†	0.04†

† Measured

‡ Provided by manufacturer

In this work, M6 PERC half solar cell (83 mm × 166 mm) with six busbars (BB) and a down-holder with six metal strips was modelled for the FEM simulation, as the experimental validation was carried using the same configuration. To reduce computational effort, a symmetry plane is applied perpendicular to the longer side of the solar cell. The ribbon comprises a round copper wire attached to the solar cell with Sn60Pb40 solder alloy. The material properties used for the simulation are summarized in Table I and Table II. In this model, the silicon solar cell and the quartz tube are treated as semi-transparent surfaces with transmissivity τ, measured as 0.12 and 0.88 respectively. The reflector is modelled as an opaque surface, and the filament and down-holders are modelled as diffuse surfaces. For opaque and diffuse surfaces, the transmissivity τ is zero.

This model does not consider the pre-heating of the solar cell at hotplates 1 and 2. Instead, the experimentally measured maximum temperature of the solar cell before the start of IR heating is used as the initial temperature, T_0, for the entire solar cell as it enters the IR heating zone. The solar cell is exposed to two radiation pulses in the IR heating zone. During the first radiation pulse, the solar cell is heated by the radiation from IR emitters 1 and 2 as it enters the IR heating zone. Subsequently, the solar cell moves under IR emitters 2, 3, and 4, where the second radiation pulse heats them. The heating from hotplate 3 is modeled using a convective boundary condition.

3 RESULTS AND DISCUSSION

The FEM model is simulated with process parameter P_{IR}= 60% for all four IR emitters and the temperature of hotplate 3, T_{HP3} = 160 °C. For validation of the simulation with experimental values, the temperature of M6 PERC half-cells was measured using thermocouples attached to the down-holder in the stringer. In this case, the initial solar cell temperature T_0 before IR heating is recorded as 121 °C. From 0 s to 1.2 s, the first radiation pulse is emitted from IR emitters 1 and 2, elevating the solar cell temperature to 176 °C. Over the next 0.8 s, the solar cell transitions to the next position inside the stringer. Between 2 s and 3.2 s, the second radiation pulse from IR emitters 2, 3 and 4 increases the temperature well above the melting liquidus temperature of the Sn60Pb40 solder (190 °C), reaching a maximum of 230 °C. After this pulse, the temperature slightly increases to a maximum of 234 °C at 3.8 s before starting to decrease within the cooling phase. Figure 2 compares the solar cell temperatures obtained from the FEM model with the measured values at position x = 36 mm / y = 71 mm in the main heating zone. The comparison shows that the FEM model accurately predicts the temperature profile during the IR soldering process.

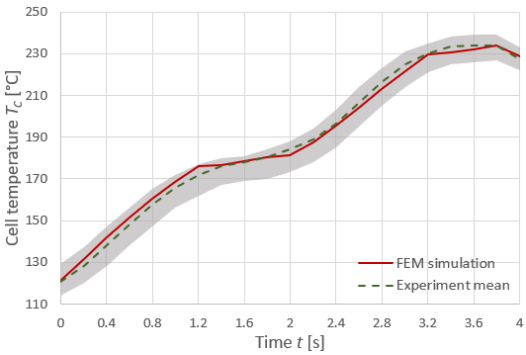

Figure 2 : Comparison of the solar cell temperature from simulation (red) and experiment (gray) during IR soldering of PERC M6 half-cells The gray area represents min./max. statistical error of N = 5 repetitions, while the dashed lines indicate the mean of the measured values.

At 3.8 s, the maximum solar cell temperature is reached. To assess temperature homogeneity across the entire solar cell, the FEM model is compared with measurements from thermocouples placed at three different positions on the solar cells. The results are presented in Figure 3. Similarly, the comparison of the measured temperatures using three thermocouples at positions x1 = 8 mm / y1 = 42 mm, x2 = 36 mm / y2 = 71 mm and x3 = 66 mm / y3 = 42 mm on the solar cells is displayed in Table III.

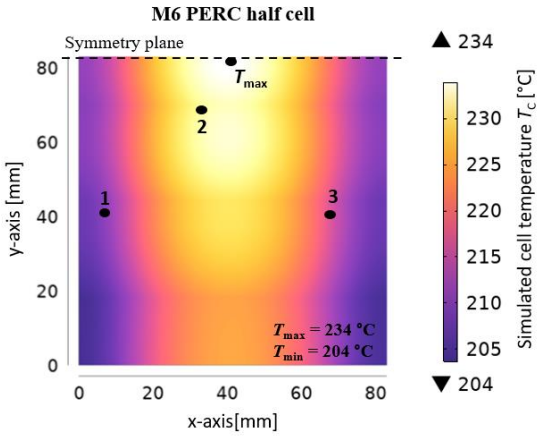

Figure 3 : a) Simulated temperature distribution on the solar cells at t = 3.8 s for different cases of process parameters measured at thermocouples 1,2 and 3.

Table III : Comparison of measured and simulated solar cell temperature at the three thermocouple positions.

Thermo-couple No.	Measured temperature [°C]	Simulated temperature [°C]	ΔT_C [K]
1	203	208	5
2	234	232	2
3	218	210	8

From the table, we can see the FEM model is able to compute the inhomogeneous temperature of the solar cell accurately, with the maximum temperature difference being (8 ± 4) K. The solar cell temperature T_C is around 30 K lower at the edges of the solar cells compared to the middle. The dominant reason for this effect is that the intensity of the radiation reduces radially as the distance from the center of the solar cell increases. Another reason is the shading and reflection of the down-holder design, as it further blocks the incident IR radiation at the edges of the solar cell. This combined effect results in higher temperature at the middle of the solar cells and relatively lower temperature at the edges of the solar cell.

4 CONCLUSION

This research introduces a novel FEM model that determines the inhomogeneous temperature distribution of solar cells during the industrial IR soldering process. The model also accounts for key factors, including the shading from the down-holder and the reflection of radiation from the IR unit reflector. Both of these elements have a significant impact on the maximum temperature reached by the solar cell during IR radiation. The model was validated by measuring the temperature at three different positions on the solar cells during the IR soldering process using thermocouples with PERC half-cells. The maximum temperature differences between the experiment and the FEM model were observed to be less than (8 ± 4) K. This FEM model can be used to determine temperature inhomogeneity during the IR soldering process for other process parameters. The model can also be easily adapted to other solar cell types, such as TopCon and silicon heterojunction (SHJ). Thus, this FEM model emerges as a reliable tool for accurately predicting temperature distribution during any industrial IR soldering process.

5 ACKNOWLEDGEMENT

The authors would like to thank the German Federal Ministry for Economic Affairs and Climate Action for the financial support within the projects “MoQa” (Grant number 03EE1140B) and “Quelle” (Grant number 03EE1172E).

6 REFERENCES

[1] A. J. Beinert, P. Romer, M. Heinrich, J. Aktaa, and H. Neuhaus, "Thermomechanical design rules for photovoltaic modules," *Progress in Photovoltaics*, vol. 31, no. 12, pp. 1181–1193, 2023, doi: 10.1002/pip.3624.

[2] M. Hertl, D. Weidmann, and J.-C. Lecomte, *Microelectronics and Packaging Conference, 2009. EMPC 2009. European*, 2009.

[3] T. Dullweber and L. Tous, *Silicon Solar Cell Metallization and Module Technology*: Institution of Engineering and Technology, 2021.

[4] J. R. Howell, M. P. Menguc, and R. Siegel, *Thermal Radiation Heat Transfer*: CRC Press, 2010.

[5] C. L. Wyatt, "Blackbody Radiation," in *Radiometric Calibration: Theory and Methods*: Elsevier, 1978, pp. 29–37.

[6] B. E. Yoldas and T. O'Keefe, "Deposition of optically transparent IR reflective coatings on glass," *Applied optics*, vol. 23, no. 20, p. 3638, 1984, doi: 10.1364/AO.23.003638.

[7] J. P. Joule, "XXXVIII. On the heat evolved by metallic conductors of electricity, and in the cells of a battery during electrolysis," *The London, Edinburgh, and Dublin Philosophical Magazine and Journal of Science*, vol. 19, no. 124, pp. 260–277, 1841, doi: 10.1080/14786444108650416.

[8] A. Jamnia, *Practical guide to the packaging of electronics: Thermal and mechanical design and analysis*, 2nd ed. Boca Raton: CRC Press, 2009.

[9] R. Strauss, *SMT Soldering Handbook*. Jordan Hill: Elsevier Science & Technology Books, 20.

[10] M. Zhao, Z. Zhou, M. Zhong, J. Tan, Y. Lian, and X. Liu, "Thermal shock behavior of fine grained W–Y 2 O 3 materials fabricated via two different manufacturing technologies," *Journal of Nuclear Materials*, vol. 470, pp. 236–243, 2016, doi: 10.1016/j.jnucmat.2015.12.042.

[11] F. Hu and S. Lucyszyn, "Modelling Miniature Incandescent Light Bulbs for Thermal Infrared ‘THz Torch’ Applications," *J Infrared Milli Terahz Waves*, vol. 36, no. 4, pp. 350–367, 2015, doi: 10.1007/s10762-014-0130-8.

[12] Y. S. Touloukian and D. P. DeWitt, *Thermophysical Properties of Matter - The TPRC Data Series. Volume 7. Thermal Radiative Properties - Metallic Elements and Alloys*. United States: New York : IFI/Plenum, 1970. Accessed: Jun. 11 2024.